PERIODICO di MINERALOGIA
established in 1930

An International Journal of
Mineralogy, Crystallography, Geochemistry,
Ore Deposits, Petrology, Volcanology
and applied topics on Environment, Archaeometry and Cultural Heritage

Glazed roman ceramic: a multi-analytical approach

Laura Medeghini [1,*], Caterina De Vito [1], Fulvio Coletti [2],
Angelica Govi [1], Lucilla Fabrizi [1], Melania Di Fazio [1], Silvano Mignardi [1]

[1] Department of Earth Sciences, Sapienza University of Rome, P.le A. Moro 5, 00185 Rome, Italy
[2] Parco Archeologico del Colosseo, Piazza di S. Maria Nova 53, 00185 Rome, Italy

ARTICLE INFO

Submitted: March 2018
Accepted: September 2018
Available on line: xxxxx 2018

* Corresponding author:
laura.medeghini@uniroma1.it

DOI: 10.2451/2018PM781

How to cite this article:
Medeghini L. et al. (2018)
Period. Mineral. 87, xx-xx

ABSTRACT

A multi-analytical approach has been applied to characterize ancient glazed ceramics from the archaeological sites of *Magna Mater* temple and *Domus Tiberiana* on the Palatine Hill (Rome, Italy) dated between the 3rd and the early 5th century AD. The aim of this work is to investigate the production technologies of the ceramic body and the glazed coating and to explore the nature and the provenance of the raw materials. Optical microscopy (OM), Fourier transform infrared spectroscopy (FTIR) and X-ray powder diffraction (XRPD) results showed that the ceramic body is composed by quartz, K-feldspar and plagioclase, fragments of igneous and sedimentary rocks. The firing temperature was estimated at about 900-1000 °C, in uncontrolled atmosphere conditions. The mineralogical assemblage of the ceramic body is consistent with a local source of the raw materials. The results of electron microscopy coupled with energy dispersive X-ray spectroscopy (SEM-EDS) showed that the glazes contain different Si/Pb ratios. In addition, X-ray fluorescence (XRF) detected the presence of Sn although its concentration does not allow defining the studied samples as tin-glazed ceramics. However, the occurrence of this element indicates an atypical Roman production, never recognized before in coeval samples from other archaeological sites.

Keywords: glazed ceramic; Palatine Hill; lead-glazed; production technology.

INTRODUCTION

Archaeometric investigations are aimed at studying the technology behind the ceramic production as well as at acquiring information that contribute to define the provenance of the raw materials (De Vito et al., 2014; Guarino et al., 2016; Medeghini et al., 2013, 2016a; Forte et al., 2018). In the case of glazed ceramics, the attention to the production technology of the glazed coatings started in the last decades aiming to reconstruct the different recipes of this particular Ceramic wares (see for example, Özçatal et al., 2014; Madkour et al., 2015; Molera et al., 2015).

The application of alkaline glazed coatings on ceramic material to obtain a brilliant and colored surface started since 1500 BC in Egypt and Mesopotamia (Tite et al., 2002; Tite, 2008) with a recipe consisting in crushed glass of alkali and silica added with coloring elements (cobalt, manganese, copper, etc.), defined frit, grounded and applied on the surfaces to form glazes (Moore and Hedges, 1975; Hedges, 1976).

In the Hellenistic and Roman ages (1st BC-1st AD centuries), the use of lead compounds (as oxides) in the glazed coatings started to be common (Wolf et al., 2003) due to the possibility to reduce the cracks giving a major optical brilliance of the surfaces. These first lead-coatings showed a chemical composition with Pb in the range 45-60%, Na_2O+K_2O less than 2% and Al_2O_3 content between 2 and 7% (Tite et al., 1998). On the basis of the variation in the chemical and mineralogical composition of glazed coatings, Walton and Tite (2010) hypothesized the diffusion of technological knowledge from the eastern Hellenistic world to the western Roman world.

The production of the glaze involved the use of lead compounds in water suspension or in the use of a clay-like suspension of lead and silica compounds, or with a frit. In all three cases, clay, rubber or starches were added to give plasticity to the suspension and facilitate the adhesion of the coating on the ceramic body.

Since 8th-9th century AD tin compounds were added in the production of the glazed coating mainly in the Iraq centers (Mason and Tite, 1997). Chemical studies by SEM-EDS of glazed ceramic fragments from Samarra, Nippur and Hira (Iraq), Susa and Siraf (Iran), Fustat (Egypt), and in Bahrain proved that the first tin opaque glazes were produced and used in Iraq (Mason and Tite, 1997).

In 9th century, the use of coating mainly composed by tin increased the amounts of tin from 3-4% to 4-9% SnO_2 in the glaze, whereas the Pb amounts were variable in the different centers of production, e.g., Bassora 6-11% PbO; Baghdad 30-45% PbO. These differences were connected to the different skill of potters and were due to the difficulty in the extraction of metal tin without Pb. This type of glaze spread throughout the Islamic world, and lately diffused into Europe during the Middle Age (1250-1700 AD) (Mason and Tite, 1997). The recipe consisted in the preparation of a suspension containing lead and silica compounds with the addition of tin oxides and alkali pre-sintered with silica compounds (Molera et al., 2001).

Among the numerous ceramic classes, the glazed Roman one, produced in the Late Antiquity (3rd - 6th century AD) and characterized by heavy coating with a dark green color, attracted the attention of archaeologists and conservator scientists. In the actual state of the study, no scientific data about this Roman ceramic class has been published because, in the past, it was usually confused with the Early Middle Ages glazed ceramic (Forum Ware) due to its similarity in the shapes and in the color of glazed coatings. The recent excavations in Rome carried out by the Soprintendenza Speciale per i Beni Archeologici di Roma in the south-west of the Palatine Hill and the latest typological and chronological studies, i.e., the re-examination of ceramic kraters from different archaeological Roman contexts, have highlighted the distinctiveness of this ceramic class. In light of this, seventeen ceramic samples with different features from the local productions have been analyzed by a multi-analytical approach including optical microscopy (OM), Fourier transform infrared spectroscopy (FTIR), X-ray powder diffraction (XRPD), electron microscopy coupled with energy dispersive X-ray spectroscopy (SEM-EDAX) and X-ray fluorescence (XRF).

The complexity and heterogeneity of ceramic bodies needed a multi-analytical approach to characterize the ceramic composition, the recipe of the glaze and the provenance of the raw material, with the final aim to provide information useful in the reconstruction of the typologies of ancient Roman glazed ceramic.

ARCHAEOLOGICAL CONTEXT

Since 1977, the archaeological excavations in the southwestern part of the Palatine Hill in Rome brought to light the remains of a large sacred architectural complex, composed of the Magna Mater and the Victoria temples (Figure 1A-B), the Auguratorium (Figure 1C) and two commercial districts. The first one (Figure 1, 1-9, F) developed along the street the clivus Victoriae (Figure 1D), on the southern side of the sanctuary, above the plateau in front of the Magna Mater temple, whereas the second one was located in the southern side of the Domus Tiberiana (Figure 1E). The sanctuary of Magna Mater, dedicated to the goddess Cybele, was built between 204 and 191 BC and then destroyed by two fires, rebuilt in the Augustus age (3 AD) and completely abandoned after 410 AD. In the southern district there was a service area composed by a bath (Figure 1F), four tabernae (Figure 1, 1-4) and four fullonicae (Figure 1, 5-9) in use from the late Antonine time to the late ancient age. The south-western side of the Domus Tiberiana was composed of a lathrine (Figure 1G) associated to a several of rooms explained like a complex for the fabric processing, used from the Hadrian period to the late 4th century AD (Coletti, 2004, 2015; Coletti and Margheritelli, 2006). The findings discovered in both areas, tuned into a trash dump, support the hypothesis that the sanctuary was used until 420 AD and probably some areas were intended for private use.

GEOLOGICAL CONTEXT

The Palatine Hill is located in the center of the city of Rome, along the eastern bank of the Tiber (Figure 2).

The geology of the Palatine Hill is made up of a sequence comprising pyroclastic and sedimentary formations of the Middle Pleistocene that characterize the province of Rome (Funiciello and Giordano, 2008 a,b).

The geomorphological structure of the area is the result of the evolution of the Roman area in the medium Pleistocene-Holocene, affected by volcanic alkaline-potassic processes of Colli Albani Volcano, of Sabatini volcanic complex and also connected to the fluvial dynamics of the river Tiber up at its mouth.

In the Wurm period (about 20-18 ka), the decrease of the sea level deeply eroded the Plio-Pleistocene stratigraphic sequence and a wide plain of marl and clays was formed (Funiciello and Giordano 2008 a,b). The increase of the sea level in the late Pleistocene-Olocene and the volcanic activity defined the actual asset of the area (Marra et al., 1998; Carboni and Iorio, 1997; Milli, 1997).

The oldest sedimentary deposit of Santa Cecilia

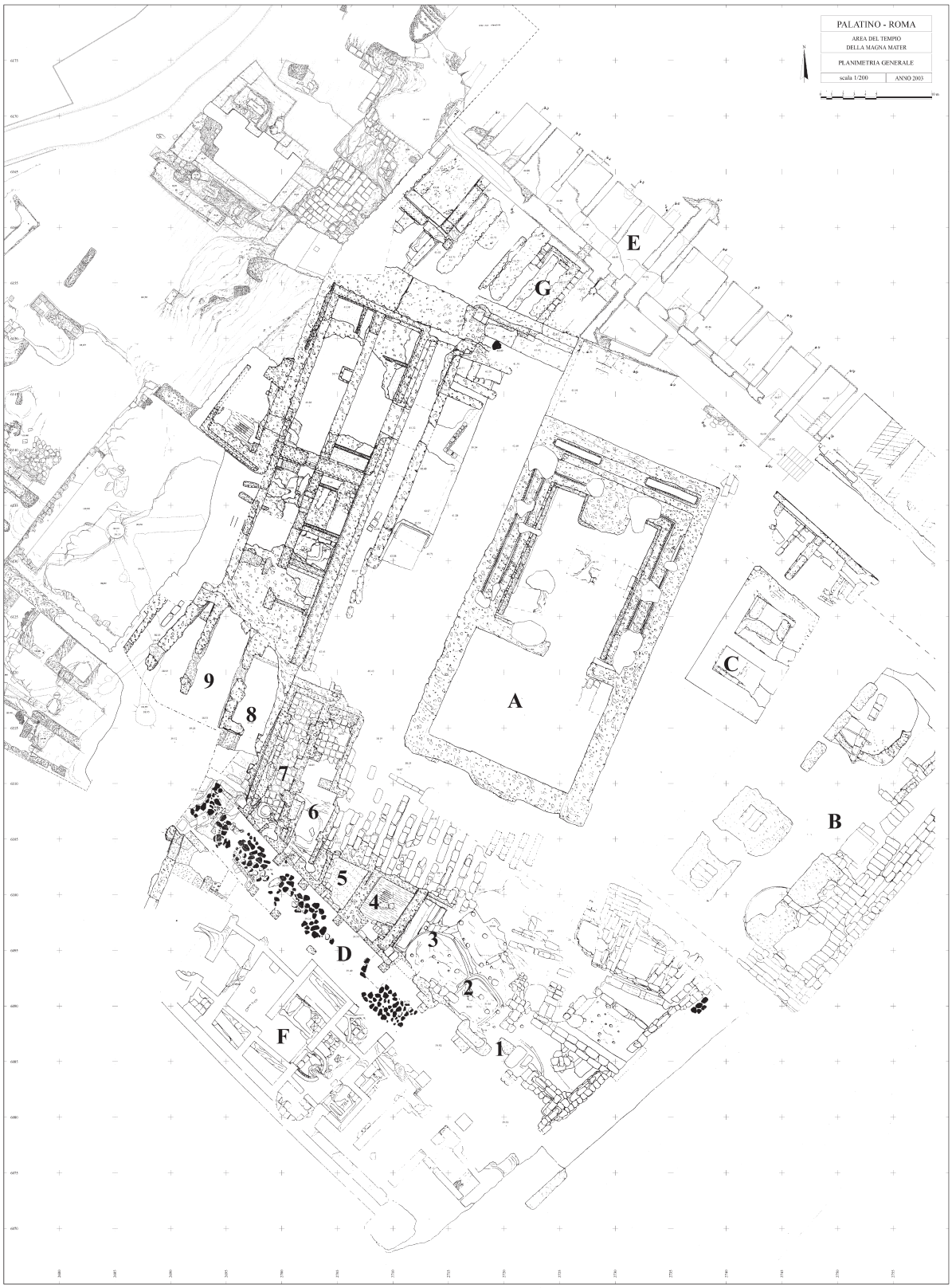

Figure 1. Map of the archaeological site (A: *Magna Mater* Temple; B: *Victoria* Temple; C: *Auguratorium*; D: *Clivus Victoriae*; E: south side of the *Domus Tiberiana*; F: Imperial baths; G: Lathrine on the south-western side of the *Domus Tiberiana*; 1-5: *Tabernae*; 6-9: *Fullonicae*).

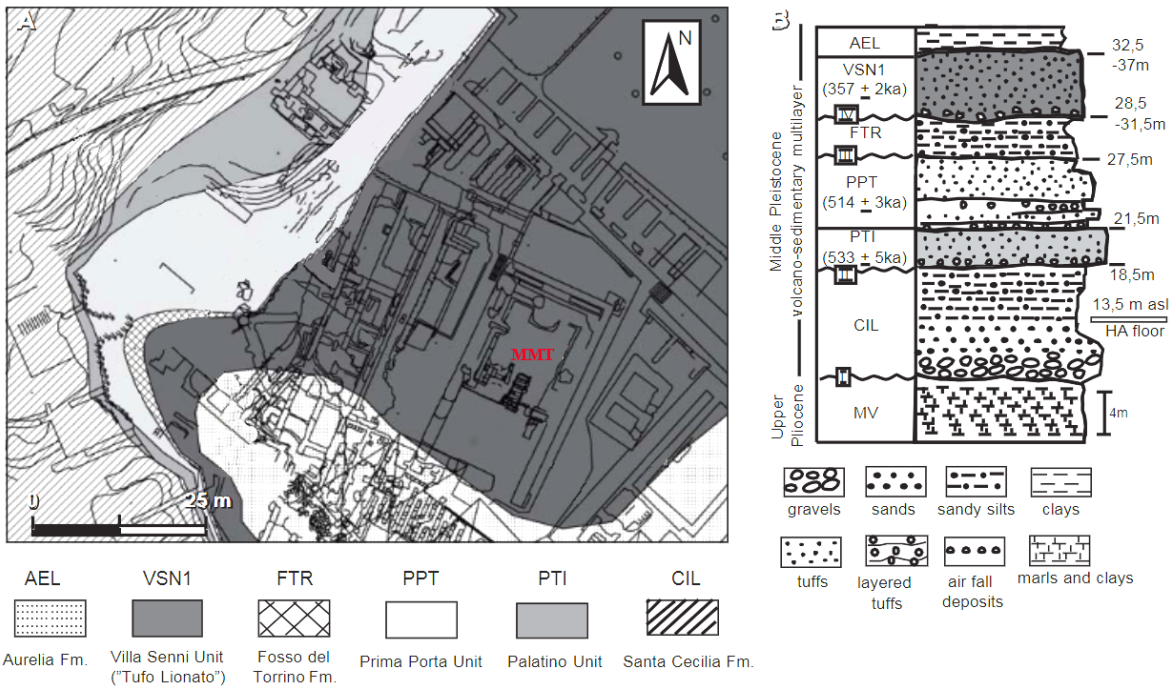

Figure 2:.A) Map of the geological setting in the south-western edge of the Palatine Hill. MMT: Magna Mater Temple. B) lithostratigraphic column according to Funiciello and Giordano (2008a,b) (modified from Di Luzio et al., 2013).

Formation of the volcano-sedimentary multilayer succession (Funiciello and Giordano, 2008b) is characterized by gravels, sands, and sandy silts with a white-grey color and mainly composed by augite, sanidine and micas. A series of volcanic unit (Palatine Unit, Prima Porta Unit and Villa Senni Unit) covers this deposit and are characterized by the presence of tuffs. The volcanic successions are interbedded by sedimentary formations of sandy silts in Fosso del Torrino Formation and clays in the most recent Aurelia Formation (Di Luzio et al., 2013).

MATERIALS AND METHODS

Materials

The seventeen ceramic fragments investigated, found mainly in the contexts dated between the late 4th and the second half of the 5th century AD, are characterized by the presence of a glazed coating ranging in color from brown, yellow to green metallic-type (Figure 3).

The ceramic samples were discovered in several of subsequent dumps inside the fullonicae in the south-western area of the Magna Mater sanctuary (Figure 1, 8-9). They have been dated between 390-410 AD (layer RZ 6705) whereas the others dated between 450 and 475-480 AD are the layers RZ 3751, RZ 5653, RZ 5654, RZ 5658, RZ 5659, RZ 5670. In the lathrine located in the south side of the Domus Tiberiana (Figure 1G), were found two contexts, between 350 and 375 AD (layer W 2418) and between 390 and 410 AD (layer W 2408).

Methods

The ceramic fragments have been analyzed using OM, FTIR, XRPD, SEM-EDAX and XRF analysis.

Petrographic analysis in thin section was performed by polarizing microscopy according to Whitbread (1995) criteria to identify the mineralogical components and define the microstructural characters and porosity using a Zeiss D-7082 Oberkochen polarized optical microscope (Department of Earth Sciences, Sapienza University, Rome, Italy).

A small quantity (1-2 mg) of each potsherd has been ground in an agate mortar for FTIR analysis and prepared using the potassium bromide pellet method. FTIR analysis was performed using a spectrometer Equinox 55 (Bruker) in the range 7500-400 cm^{-1} with a resolution of 2 cm^{-1} and 256 scans (IGG-CNR section of Rome, Department of Earth Sciences, Sapienza University, Rome, Italy). Origin Pro software was used for smoothing data and correction of baseline; the peak identification was made possible thanks to the bibliographic comparison (De Benedetto et al., 2002).

A Siemens D5000 diffractometer (Department of Earth Sciences, Sapienza University, Rome, Italy) with CuKα

Figure 3. Macroscopic images of representative samples: TMM98RZ5670, TMM98RZ5892, TMM98RZ5653, TMM86W2418, TMM86W2906 (from left to right).

radiation is used to identify the mineralogical composition of the samples in operating conditions of 40 kV and 30 mA, in the range of 3°-60° 2θ, at a speed of 1°/min and 2s/step, 1° diverging slide, slide receiver of 0.1 mm and sled antiscatter of 2°. The data collected in terms of intensity and diffraction angles were processed with XPowder 12 software.

Thin sections of ceramic samples were metalized with graphite and SEM investigations carried out using an electron microscope FEI Quanta 400 (Department of Earth Sciences, Sapienza University, Rome, Italy), equipped with the unit of EDAX microanalysis to define the microstructure of the ceramic samples and the chemical composition and morphology of the glazed coating.

Finally, qualitative chemical analysis was performed using a portable micro-XRF Artax 200 Bruker AXS (Department of Chemistry and Geology, University of Modena and Reggio Emilia, Italy). The instrumental set up includes a detector (SDD Silicon Drift Detector) and an X-ray generator equipped with a molybdenum source. This arrangement makes possible the analysis of XRF punctual type with a spatial resolution of less than 70 μm. The instrument is equipped with a laser sighting system and a CCD camera, powered at 50 kV and 700 mA in air and without filters.

RESULTS AND DISCUSSION

Ceramic body

Petrographic analysis

Three homogenous petrographic groups (fabrics) have been identified and the detailed description of their features is reported in Table 1.

Fabric A includes samples TMM07RZ3751, TMM93RZ5653 and TMM98RZ5670, which contain very few sedimentary carbonate rock fragments, such as limestone.

Fabric B has been divided into three sub-groups. The sub-groups B1 and B2 are both characterized by a diffuse presence of quartz but are distinguishable by the different particle size. The group B1 (TMM98RZ5892) is characterized by the dominant presence of quartz with shape from angular to sub-angular and fine particle size (0.2-0.4 mm) and the minor presence of iron oxides. The group B2 (TMM98RZ5653, TMM98RZ5654, TMM93RZ3751, TMM07RZ6602) is characterized by the frequent presence of quartz with shape from angular to sub-angular and larger grain size (0.4-0.6 mm). The group B3 (TMM86W2418, TMM98RZ5658, TMM86W2408, TMM07RZ6705, TMMRZ3751, TMM07RZ6705*) shows a frequent presence of siliceous rock of flint type.

Fabric C (TMM86W2906, TMM87W2906, TMM98RZ5610) is characterized by the presence of inclusions of basaltic rocks from sub-angular to sub-rounded.

FTIR Analysis

Representative samples have been studied using FTIR to identify the presence of inorganic and organic compounds (Table 2).

FTIR spectra allowed identifying quartz and K-feldspar in all the analyzed samples (Figure 4). Indeed, samples show a broad band at 1200-800 cm^{-1} due to the asymmetric stretching of the Si-O silicate, even if the intensity of these bands varies from sample to sample. Quartz is present in

Table 1. Microscopic features of samples analyzed.

Sample	Pores	Matrix	Inclusions	Glaze	Fabric
TMM98RZ5670	5% micro-vescicles, meso-vughs	65% not calcareous. homogeneous	30% *frequent*: quartz; *common*: fragments of siliceous sedimentary rocks, nodules of iron oxides *very few*: fragments of calcareous sedimentary rocks	One margin, transparent, bubbles and inclusions inside	A
TMM93RZ5653	5% micro-vescicles, meso-vughs	45% not calcareous. heterogeneous	50% *frequent*: quartz; *common*: fragments of siliceous sedimentary rocks *very few*: fragments of calcareous sedimentary rocks, nodules of iron oxides	Both margins, transparent-gray, bubbles and inclusions inside	A
TMM99RZ5653	5% micro-vescicles, meso-vughs	55% not calcareous. heterogeneous	40% *frequent*: quartz; *few*: nodules of iron oxides *very few*: fragments of calcareous sedimentary rocks	Both margins, transparent-gray	A
TMM07RZ3751	5% micro-vescicles, micro- meso-vughs	55% not calcareous. heterogeneous	40% *common*: quartz; *few*: nodules of iron oxides *very few*: fragments of siliceous and calcareous sedimentary rocks	Both margins, transparent-gray, bubbles and inclusions inside	A
TMM99RZ5515	5% micro-vescicles, meso- macro- vughs	45% not calcareous. homogeneous	50% *dominant*: quartz; *few*: fragments of siliceous sedimentary rocks, nodules of iron oxides	One margin, transparent-gray	B1
TMM98RZ5892	5% micro-vescicles, micro- meso-vughs	45% not calcareous. homogeneous	50% *dominant*: quartz; *common*: fragments of siliceous sedimentary rocks *few*: iron oxides	One margin, transparent-gray	B1
TMM98RZ5653	5% micro-vescicles, micro- meso-vughs	45% not calcareous. homogeneous	50% *frequent*: quartz; *common*: fragments of siliceous sedimentary rocks, nodules of iron oxides	One margin, transparent-gray	B2
TMM98RZ5654	5% micro-vescicles, meso-vughs	45% not calcareous. homogeneous	50% *frequent*: quartz; *common*: fragments of siliceous sedimentary rocks, nodules of iron oxides	Both margins, transparent-gray	B2
TMM93RZ3751	5% micro- meso- vescicles, meso-vughs	45% not calcareous. homogeneous	50% *frequent*: quartz; *common*: fragments of siliceous sedimentary rocks, nodules of iron oxides	Both margins, transparent-gray	B2
TMM07RZ6602	10% micro- meso- vescicles, micro- meso-vughs	40% not calcareous. homogeneous	50% *frequent*: quartz; *common*: nodules of iron oxides *few*: fragments of siliceous sedimentary rocks	Both margins, transparent-gray	B2
TMM86W2418	5% micro-vescicles, meso-vughs	70% not calcareous. homogeneous	25% *frequent*: quartz, fragments of siliceous sedimentary rocks *very few*: nodules of iron oxides	One margin, transparent-gray bubbles and inclusions inside	B3

Table 1. ... Continued

Sample	Pores	Matrix	Inclusions	Glaze	Fabric
TMM98RZ5658	5% micro-vescicles, micro- meso-vughs	60% not calcareous. heterogeneous	35% *frequent*: fragments of siliceous sedimentary rocks *common*: quartz, nodules of iron oxides	Both margins, transparent-gray	B3
TMM86W2408	5% micro-vescicles, meso-vughs	50% not calcareous. heterogeneous	45% *frequent*: fragments of siliceous sedimentary rocks *common*: quartz, nodules of iron oxides	One margin, transparent-gray	B3
TMM07RZ6705	1% micro-vescicles	64% not calcareous. homogeneous	35% *frequent*: fragments of siliceous sedimentary rocks, nodules of iron oxides *few*: quartz	One margin, transparent-gray	B3
TMMRZ3751	5% micro- meso- vescicles	55% not calcareous. homogeneous	40% *frequent*: fragments of siliceous sedimentary rocks, nodules of iron oxides *common*: quartz	One margin, transparent-gray	B3
TMM98RZ5659	5% micro-vescicles, micro- meso-vughs	55% not calcareous. heterogeneous	40% *frequent*: fragments of siliceous sedimentary rocks *common*: quartz, nodules of iron oxides	Both margins, transparent-gray	B3
TMM07RZ6705*	5% micro-meso vescicles, micro- meso vughs	55% not calcareous. homogeneous	45% *common*: quartz, fragments of siliceous sedimentary rocks *few*: nodules of iron oxides	Both margins, transparent-gray bubbles and inclusions inside	B3
TMM86W2906	5% micro-vescicles	75% not calcareous. heterogeneous	20% *common*: quartz, nodules of iron oxides *very few*: fragments of basaltic rocks, feldspar, plagioclase, pyroxene	Both margins, transparent-gray bubbles inside	C
TMM87W2906	5% micro-vescicles	70% not calcareous. homogeneous	25% *common*: quartz, nodules of iron oxides *very few*: fragments of basaltic rocks and siliceous sedimentary rocks, feldspar, plagioclase, pyroxene	Both margins, transparent-gray inclusions inside	C
TMM98RZ5610	5% micro-vescicles	70% not calcareous. homogeneous	25% frequent: quartz *common*: nodules of iron oxides *few*: fragments of basaltic and siliceous sedimentary rocks, feldspar, plagioclase, pyroxene	Both margins, transparent-gray	C

all the ceramics and has been identified in each sample in high amounts. Its presence is marked by the main Si-O stretching band at 1076 cm^{-1}, the doublet at 796 cm^{-1} due to the bending Si-O, the peak at 775 cm^{-1} due to stretching Si-O-Si stretching, and the weak bands at about 694, 512 cm^{-1} (Legodi and de Waal, 2007; Shoval and Paz, 2015).

Feldspars occur as plagioclase and alkali feldspar. Albite has been identified by the peaks at 1025, 991 and 580 cm^{-1}, whereas anorthite was characterized by peaks at 732 and 665 cm^{-1}. Alkali feldspars have been identified in all the ceramic samples by the peaks at 1135, 1029, 723, 644, 586, 539, 433 and 462 cm^{-1}.

In addition, diopside (peaks at 962, 863, 673 cm^{-1}), gehlenite (peaks at 987, 1051 cm^{-1}) and muscovite (peaks at 617, 931, 989 cm^{-1}) have been identified, although in very low amounts. In addition, calcite in low amounts was detected by its characteristic band at 1428 cm^{-1} in samples TMM98RZ5670 and TMM93RZ5653 (Medeghini et al., 2016b).

Table 2. Mineral phases and abundances based on the intensity of absorption bands (*** abundant, ** present, * scarce) identified by FTIR analysis (Qtz: quartz, Kfs: K-feldspar, Pl: plagioclase, Cal: calcite, Di: diopside, Ms: muscovite, Gh: gehlenite).

	Fabric	Qtz	Kfs	Pl	Cal	Di	Ms	Gh
TMM98RZ5670	A	***	**	**	*			
TMM93RZ5653	A	***	*	**	*	**		
TMM98RZ5892	B1	***	**	**				
TMM98RZ5653	B2	***	**					
TMM86W2418	B3	***	**			*	*	
TMM98RZ5658	B3	***	**	**				
TMM86W2906	C	***	*	**		**	**	
TMM87W2906	C	***		**		**	**	

XRPD analysis

Samples analyzed by FTIR have also been studied by XRPD with the purpose to better identify each mineralogical phase. The identified mineral phases and their abundances are reported in Table 3.

The intensity of the peaks in all samples showed abundant quartz, and diffuse K-feldspar, whereas the abundance of other mineral phases such as plagioclase, diopside, gehlenite, muscovite, hematite, and epidote varies from sample to sample (Figure 5). In addition, calcite was identified in traces only in two samples (TMM98RZ5670, TMM93RZ5653), in agreement with FTIR results.

SEM-EDS analysis

SEM-EDS analysis shows that the samples are characterized by the presence of many inclusions and appear to be very similar to each other. In particular, the most diffuse mineral phase in all the analyzed samples is quartz.

Plagioclase has been also identified; however, it is difficult to distinguish the intermediate term of the albite-anorthite series. It is reasonable to hypothesize the presence of andesine and labradorite plagioclase typical in the intermediate and basic rocks. In the fragments of basaltic rocks rare apatite, titanium and iron oxides (probably ilmenite) were also identified (Figure 6).

SEM-EDS analysis also allows defining the chemical composition of the matrix that is similar in all the samples and characterized by high amount of Si, minor of Al, Mg, Na, K, Fe and Ca, variable from samples to samples.

XRF analysis

XRF analysis was applied to better define the chemical composition of the matrix of all the analyzed samples. In the ceramic body the results revealed the presence of high concentrations of Fe and Ca, small amounts of Mn, Zn, whereas appreciable amounts of Sn were not measured.

The occurrence of Cu indicated that such element was used for coloring the ceramics. Zn is always associated

Table 3. Mineral phases and semi-quantitative evaluation by XRPD (*** abundant, ** present, * scarce, tr traces) identified by XRPD analysis (Qtz: quartz, Pl: plagioclase, Kfs: K-feldspar, Gh: gehlenite, Ms: muscovite, Cpx: clinopyroxene, Hem: hematite, Ep: epidoto, Cal: calcite).

	Fabric	Qtz	Pl	Kfs	Gh	Ms	Cpx	Hem	Ep	Cal
TMM98RZ5670	A	***	**	*	tr	tr	tr			tr
TMM93RZ5653	A	***	**	*			*	*		tr
TMM98RZ5892	B1	***	**	**						
TMM98RZ5653	B2	***		**		*				
TMM86W2418	B3	***		**			*	*		
TMM98RZ5658	B3	***	**	*	*					
TMM86W2906	C	***	**	*	tr	*	*	*	*	
TMM87W2906	C	***	**	*	tr	tr	tr	*	*	

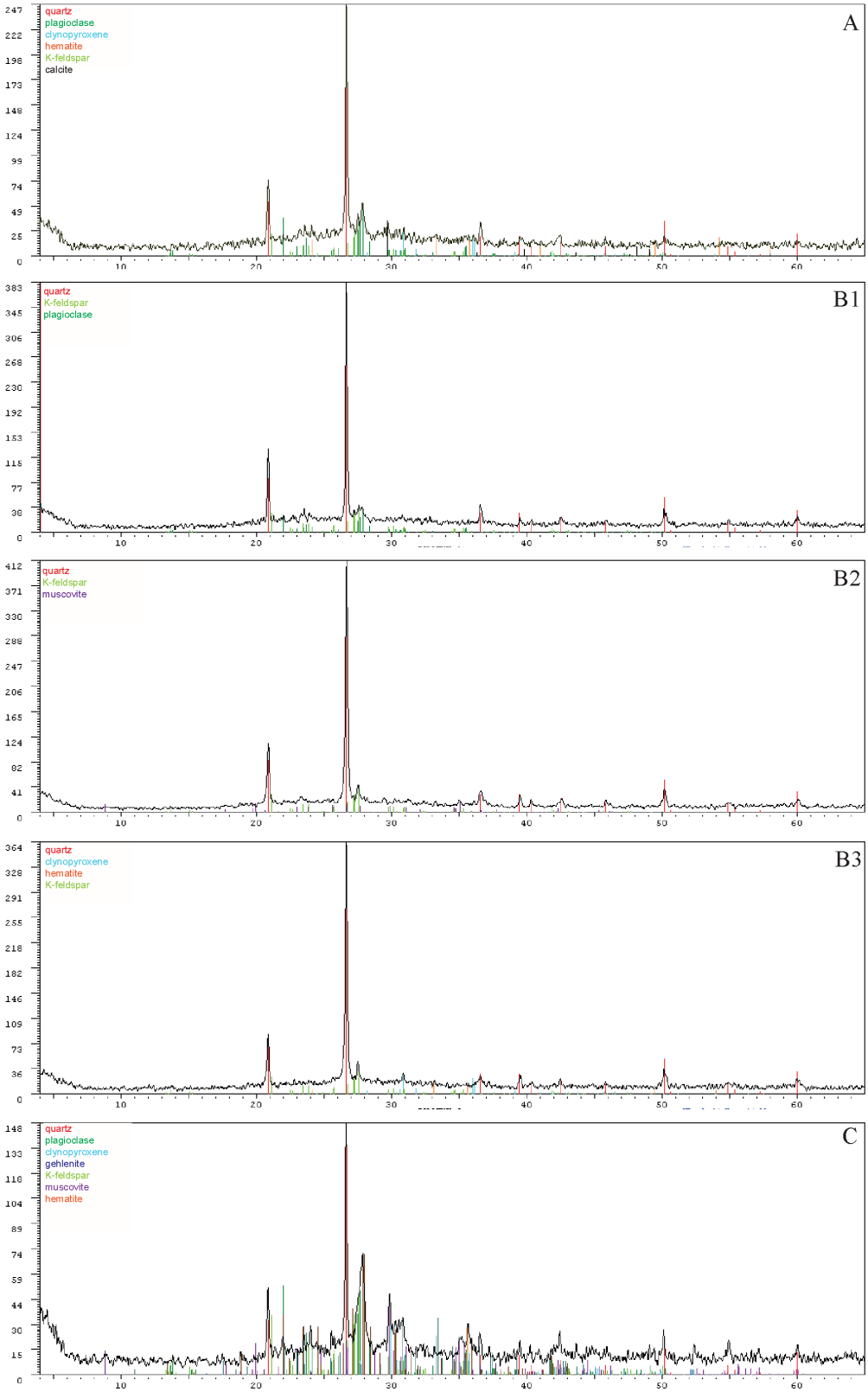

Figure 4. Representative XRD patterns: fabric A sample TMM93RZ5653, fabric B1 sample TMM98RZ5892, fabric B2 sample TMM98RZ5653, fabric B3 sample TMM86W2418, fabric C sample TMM86W2906.

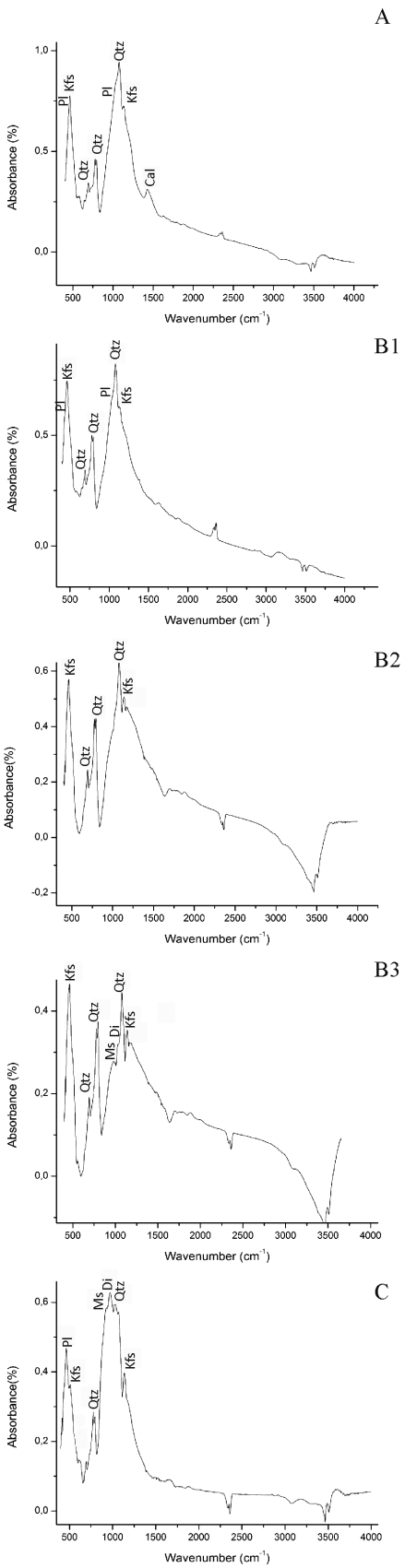

with Cu. Finally, the presence of Pb in the ceramic body may be due to contamination from the glassy coating present on the ceramic body.

Glazed coating

Petrographic analysis

OM analysis provided preliminary information about the glazed coating. The color is transparent-gray in plane polarized light (PPL) and from green to dark under crossed polarized light (XP); no optical activity was observed. It is compenetrate into the body, and some bubbles were identified inside (Table 1). Moreover, some silica inclusions (mainly quartz), with angular shape, not completely melt, are present in the coating.

SEM-EDS analysis

Chemical investigation performed with SEM-EDS analysis allowed to define the stratigraphic sequence of the elements that make up the surface coating of the ceramic.

SEM images show that the thickness of the glaze varies from 100 to 230 μm for the internal and from 100 to 350 μm for the external surface.

EDS analysis has been performed along the thickness of the coating to check any compositional variations. The bulk composition is generally homogeneous along the cross section, showing high concentrations of Pb, as well as Ca and Al, and moderate contents of Mg, Na and K. Chromophore elements such as Cu and Fe are also present.

In addition to these elements, in a very small area of the external coating, a small amount of Sn was found in sample TMM98RZ5658.

TMM87W2906 and TMM98RZ5610 sample show a layered structure of the glazed coating. EDS spectra showed that the composition of this layered structure is similar to those of the glaze, with layer containing high amount of Pb, Ca and P alternated with Si-rich and Al-bearing layers (Figure 7).

XRF analysis

The identification of Sn in sample TMM98RZ5658 by SEM-EDS analysis needed a depth investigation of the chemical composition of the glaze by XRF. The samples were divided into 3 groups considering the presence or absence of Sn in the coatings. The first group consists of the sample TMM98RZ5892 and TMM98RZ5658

Figure 5. Representative FTIR spectra with the different assignments. Fabric A sample TMM98RZ5670, fabric B1 sample TMM98RZ5892, fabric B2 sample TMM98RZ5653, fabric B3 sample TMM86W2418, fabric C sample TMM86W2906.

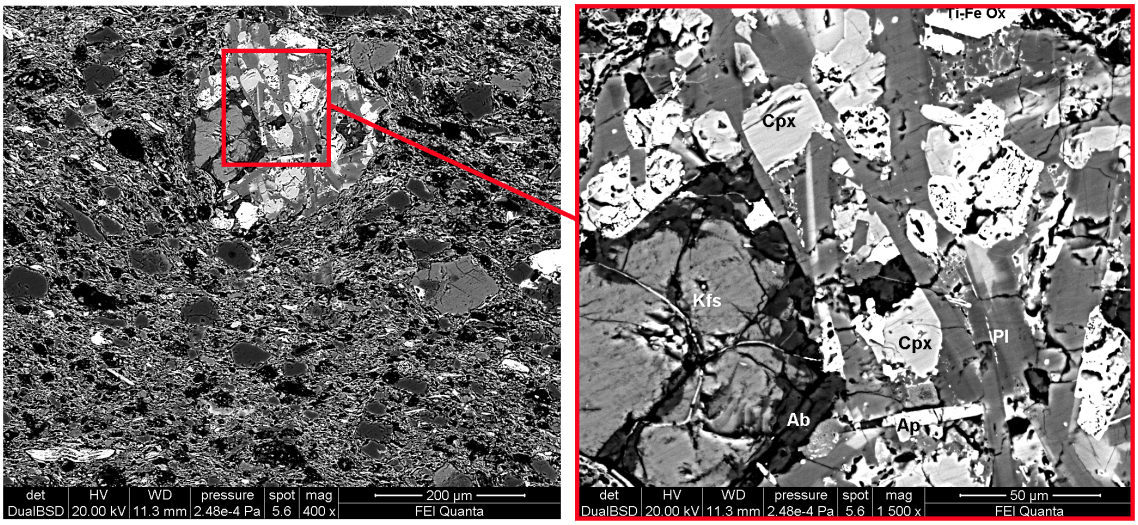

Figure 6. BSE images of a fragments of basaltic rocks in sample TMM87W2906 including clinopyroxene (Cpx), K-feldspar (Kfs), plagioclase (Pl), albite (Ab), apatite (Ap), titanium and iron oxides (Ti-Fe ox).

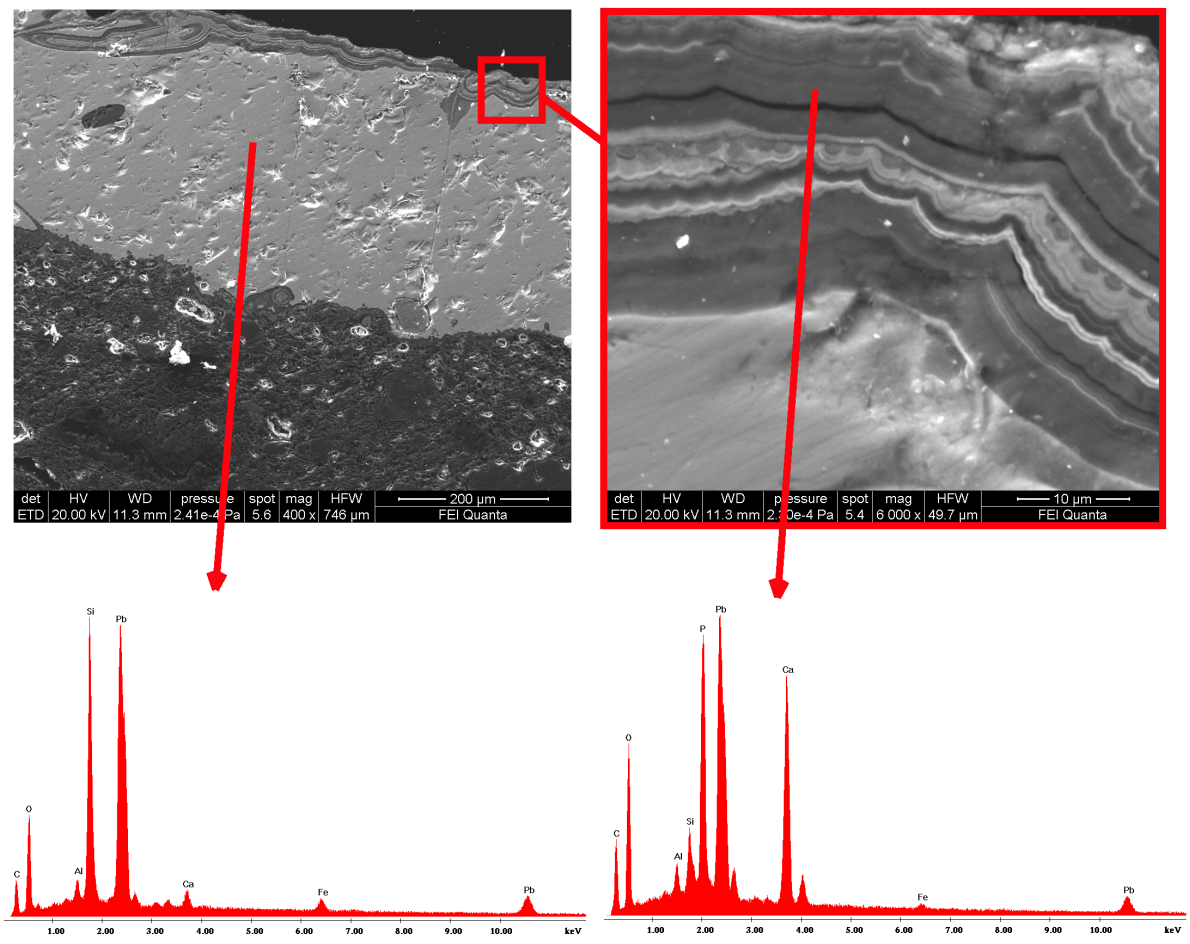

Figure 7. SE images and EDS spectra of glazed coating of sample TMM87W2906 showing a layered structure due to devitrification processes of the surfaces of the sample.

and it is characterized by moderate contents of Sn, high amounts of Pb, minor amounts of Fe, Cu and Ca. The second group (samples TMM93RZ3751, TMM98RZ5653, TMM86W2418, TMM07RZ6602, TMM98RZ5654, TMM07RZ3751, TMM07RZ6705, TMM86W2408, TMMRZ3751, TMM98RZ5670, TMM07RZ6705*, TMM93RZ5653) shows low contents of Sn, high amounts of Pb, moderate amounts of Fe, and modest contents of Cu and Ca.

Finally, the third group consists of the samples TMM87W2906, TMM86W2906, TMM98RZ5610 and it is characterized by levels of Sn below the detection limit of the instrument. The glaze in these samples shows high amounts of Pb, moderate amounts of Fe and modest contents of Cu.

DISCUSSION

Ceramic body

Chemical and mineralogical composition of the ceramic body is similar in all the samples, differing only on the basis of the different amounts of mineral phases. The ceramic body is mainly composed by silicate minerals such as monocrystalline quartz, K-feldspar, plagioclase; in addition, fragments of igneous and sedimentary rocks are identified. Quartz is the most abundant mineral phase and represents the major component of the raw material used in the ceramic production. It could be naturally present into the starting clay or added by the potter to modify the plasticity of the clay (Forte and Medeghini, 2017), but it is very difficult to distinguish the two cases (Papachristodoulou et al., 2006). However, the presence of rounded inclusions, the unimodal grain size distribution (Quinn, 2013) and the absence of grog (Riederer, 2004) support the hypothesis that the entire components in the clay were naturally present in the raw material.

K-feldspar and plagioclase are both identified in the matrix. SEM-EDS analysis revealed the presence of andesine/labradorite plagioclase, supporting the contribution of basaltic rocks fragments as igneous inclusions by OM.

Some samples show also the presence of fragments of sedimentary rocks, mainly siliceous as flint-type, rarely carbonaceous. Indeed, analytical methods revealed the presence of calcite in traces only in fabric A samples, where very few fragments of carbonaceous sedimentary rocks are identified, suggesting the hypothesis that it was naturally present in the starting raw material. This is confirmed by FTIR spectra showing the band of primary calcite, due to the stretching C-O, at about 1428 cm^{-1}. Indeed, according to Shoval and Nathan (2011) and Fabbri et al. (2014), secondary calcite resulted in a rounded and asymmetric band between 1430 and 1450 cm^{-1}, due to the lower size of crystals and the lower degree of crystallinity,

Clinopyroxene (augite) is identified only in samples of fabric C which contain fragments of basaltic rocks. The percentage and the size of these inclusions suggest that they were naturally present in the starting clay and not added as tempers.

Other minerals identified as rare phases are ilmenite and apatite, which probably represent accessory minerals of basaltic rocks.

The results allow hypothesizing that the ceramics analyzed were produced using a starting clay, not calcareous, characterized by the presence of quartz, K-feldspar, clinopyroxene and fragments of volcanic rocks (with plagioclase feldspar, clinopyroxene, iron and titanium oxides and apatite). The mineralogical composition is consistent with the local geology suggesting a supply of the raw material in the Roman area.

Moreover, our results highlight a relationship among vases shapes and inclusions found in the matrix. For example, *patere ansate* and *amphorae*, belonging to fabric B2, are characterized by the occurrence of large quartz crystals. These shapes were usually used as liquid containers during the rituals; therefore, a starting raw material with big inclusions of quartz assured a strong structure avoiding cracks or fractures (Tite et al., 2001).

The color of matrix varies from red to gray; the samples with red or pink matrix were probably fired in oxidizing atmosphere, whereas samples with gray or dark color are hypothesized fired in reducing conditions or in reduced atmosphere during cooling. In some samples, the color varies along fracture probably connected to a not complete firing due to a short time, low temperature or not controlled fugacity of oxygen. The variability in the color of matrix is related to a not complete control during the phases of firing or cooling, or, in general, to conditions of firing not homogeneous (Lofrumento et al., 2004).

The mineralogical composition of ceramic samples analyzed allows indicating a firing range between 850 and 1000 °C, due to the presence of gehlenite, diopside and hematite. In particular, the presence of gehlenite in some samples would indicate a firing temperature close to 900 °C.

However, small amounts of calcite, identified as primary phase in some samples, suggest that they were fired at temperature close to the upper limit of decarbonation. Indeed, calcite starts to decompose at about 650 °C (Medeghini and Nigro, 2017) into CaO and CO_2. The oxides react with silica and alumina from the breakdown of clay minerals forming new phases such as calcium silicate or calcium aluminum silicates (Ballirano et al., 2014; Medeghini et al., 2016c). In particular, gehlenite is stable in the range 800-950 °C (De Benedetto et al., 2002; De Vito et al., 2015) and it is formed according to the reaction:

$$2CaO + Al_2O_3 + SiO_2 \rightarrow Ca_2Al_2SiO_7 \quad (1)$$

Diopside forms at about 850 °C (Bersani et al., 2010) following the reaction:

$$CaO + MgO + 2SiO_2 \rightarrow CaMgSi_2O_6 \quad (2)$$

The co-occurrence in the same sample of calcite and newly formed minerals indicates an incomplete reaction among clay minerals and calcite. This could be due to low temperature and/or short time of firing. Numerous studies (Maniatis and Tite, 1981; Riccardi et al., 1999; Trindade et al., 2009) suggest that calcareous clay starts to decompose at lower temperature than that poor of carbonates because Ca and Mg can act as flux agents.

Glazed coating

The detailed characterization of the glazed coating is fundamental to help in the typological archaeological classification, to reconstruct the complex productions developed in the atelier, to identify the origin of these productions and the related technological knowledge (Capelli and Cabella, 2004; Berti et al., 2006).

SEM-EDS analysis allowed the definition of chemical composition of glazed coating as well as the observation of post-depositional alteration that interferes with a naked-eyes observation.

The coatings have a thickness between 100 and 350 μm, and the thicker ones are characterized by the occurrence of bubbles probably due to the CO_2 produced after the thermal decomposition of organic matter added to the frit to promote the adhesion to the ceramic body (Özcatal et al., 2014). However, the high viscosity of the glaze prevents the bubbles reach the surface staying inside the glazed layer (Özcatal et al., 2014).

Chemical analysis proves that glazed coatings were composed by silica, lead as flux agent and other elements such as Na, K, Al and Ca. Therefore, the studied samples can be defined as high lead glazed ceramics (Tite et al., 1998). Moreover, the chemical composition suggests a firing temperature in the range 900-1000 °C, compatible with that of the ceramic body.

The green color of the majority of the samples is due to the presence of Cu, whereas the yellow and dark yellow color can be related to Fe in different oxidation state (Molera et al., 2001; De Vito et al., 2017, 2018).

However, SEM-EDS analysis highlighted also the presence of SnO, usually used as opacifier in glazes. The addition of Sn determines microcrystalline or cryptocrystalline inclusions with light color, not identified in our samples by OM analysis. On the contrary, the glazes appear transparent in PPL and gray-opaque in XP, due to the presence of lead oxide (Cuomo di Caprio, 2007). Indeed, SEM-EDS analysis revealed the presence of Sn only in a small area in one sample, whereas XRF data show that a small amount of Sn is present in almost all the samples. In particular, this element was detected in the majority of samples collected by the Magna Mater temple, dated in the range 4^{th}-5^{th} century AD with dark green glaze. On the contrary, Sn was not detected in the samples with yellow or light green color from the service areas of the Domus Tiberiana (3^{rd}-5^{th} century AD). The presence of Sn could suggest a particular ceramic production for Magna Mater temple samples; however, the low amount of Sn detected in our samples does not permit to opacify the coating not allowing us to define these coatings as tin-lead glazes.

The occurrence of quartz inclusions not completely melt into the coating suggests the use of ground frit or quartz sand (Tite et al., 1998). The angular shape observed support the hypothesis of the application of a frit composed by lead oxide and silica.

Optical microscopy shows the glazed coating is compenetrate into the ceramic body as the result of a single cycle of firing. On the contrary, electron microscopy did not detect newly formed minerals developed at the interface glaze/ceramic body, supporting the hypothesis of two different stages of firing with the application of the frit at the end of the first firing stage. However, the formation of these new minerals (K-feldspars enriched in Pb as reported by De Vito et al., 2017) depends on different factors such as the amount of PbO, the maximum firing temperature and the cooling rate (Molera et al., 2001).

The reduced variability of K, Al and Fe along the thickness of the glaze, the irregular shape of the glaze at the interface glaze/ceramic body, the variability of color of glazes and ceramic bodies further support the hypothesis of a single firing cycle (Tite et al., 1998).

Finally, traces of devitrification processes on the surfaces of samples, resulting in the typical leached layer structure (Garofano et al., 2015), are shown by SEM images. These layers are due to the leaching of ions in the glaze and the interaction with the burial environment, i.e H^+ from fluid medium, Ca^{2+} and Pb^{2+} from the glaze, and P from the environment. The process of leaching and the subsequent local precipitation of secondary phases depend on pH, Eh, concentration of ions in the solution (Silvestri et al., 2005; Doménech-Carbó et al., 2006; Garofano et al., 2015). These alteration structures determine volume and structural changes including cracking on the surface that could favor further alterations. The alterations were identified in the samples from the service areas of Domus Tiberiana close to the cloaca, a buried environment enriched in P.

The results of this study support the hypothesis that the ceramic fragments from the Magna Mater temple

represented an atypical ceramic Roman production (Coletti, 2012). The peculiar shapes of the vases, the presence of low percentage of Sn in the glaze and the application of lead oxides with the addition of silica, differently from other coeval samples from Carlino (Udine, Italy) (Magrini and Sbarra, 2005; Walton and Tite, 2005), further validate the traits of specialization and distinctiveness of this production, probably due to the particular use connected to the liturgical practices of the eastern cults in Rome (i.e., Mythra and Cybele). Indeed, these productions differ from those that were produced for army or rural environments (such as from Carlino) (Capelli et al., 2007) and that never achieved the technical and morphological refinement found in the Roman glazed samples.

CONCLUSIONS

The multi-analytical approach applied in the study of glazed ceramic from the archaeological sites of Magna Mater temple and the service areas of Domus Tiberiana on the Palatin Hill provides information about the technological process of production, the nature of the raw materials, the kind of mixture prepared for the coating, the application mode, the superficial treatments and the firing conditions.

The ceramic body is composed by quartz, K-feldspar, plagioclase, fragments of igneous and sedimentary rocks. The mineralogical and petrographic composition is consistent with lithotypes outcropping in the Palatine area, suggesting a local production for this particular ceramic production. The occurrence of newly formed minerals along with primary calcite suggests a firing temperature in the range 900-1000 °C in oxidizing or reducing conditions. The variability in the color of the matrix observed in the majority of the samples supports the hypothesis of incomplete reactions due to firing or fast cooling or not controlled.

The glazed coatings are mainly composed by silica derived from quartz sand and lead as flux agent. In addition, Fe and Cu are responsible for the different green and yellow color of these glazes.

The recipe consisted in the preparation of a frit composed by silica and lead oxides, in water and applied on the ceramic body, then fired in one cycle. The vitrification temperature of glazed coating is compatible with that of the firing of the ceramic body. In samples with dark green color from the Magna Mater temple, the analysis showed the presence of low amount of tin. The low percentage suggests that this element could be part of the starting raw material, different from the productions found in the Domus Tiberiana. For this reason, an atypical and prestigious production is hypothesized, probably connected to the Mytra cult.

The ceramic samples discovered in the service areas of the Domus Tiberiana are characterized by an external altered layer superimposed on the glaze. The presence of P in these layers suggests ions exchanges between the ceramics and the burial environment.

ACKNOWLEDGEMENTS

This research was funded by Sapienza University of Rome, Italy. It was part of the thesis of AG under the guidance of SM. LM designed the study, contributed in the experiments and analysis and wrote the manuscript with SM and CDV, considering also inputs from other authors.

REFERENCES

Ballirano P., De Vito C., Medeghini L., Mignardi S., Ferrini V., Matthiae P., Bersani D., Lottici P.P., 2014. A combined use of optical microscopy, X-ray powder diffraction and micro-Raman spectroscopy for the characterization of ancient ceramic from Ebla (Syria). Ceramics International 40, 16409-16419.

Bersani D., Lottici P.P, Virgenti S., Sodo A., Malvestuti G., Botti A., Salvioli-Mariani E., Tribaudino M., Ospitali F., Catarsi M., 2010. Multi-technique investigation of archaeological pottery from Parma (Italy). Journal of Raman Spectroscopy 41, 1266-1271.

Berti G., Capelli C., Gelichi S., 2006. Trasmissioni tecniche tra XII e XIII secolo nel Mediterraneo: il contributo dell'archeometria nello studio degli ingobbi. In: Atti del IV Congresso di archeologia medievale, Abbazia di San Galgano (Chiusdino-Siena), 26-30 settembre 2006. (Eds.) R. Francovich, M. Valenti, All'Insegna del Giglio, Firenze, 455-460.

Capelli C. and Cabella R., 2004. Note sulla caratterizzazione dei rivestimenti delle ceramiche medievali. In: Metodi e pratica della cultura materiale. Produzione e consumo dei manufatti. (Ed.) E. Giannichedda, Bordighera Istituto di studi liguri, 125-132.

Capelli C., Cabella R., Piazza M., 2007. The Late Roman glazed pottery production in Eastern Alpine area and Danubian provinces: archaeometric analyses on fabrics and glazes. In: La ceramica invetriata tardoromana nell'arco alpino orientale e nelle province danubiane. Primi risultati di un progetto internazionale. Atti del I incontro Internazionale di Archeologia a Carlino. (Eds.) C. Magrini, F. Sbarra, Carlino, 71-109.

Carboni M.G. and Iorio D., 1997. Nuovi dati sul Plio-Pleistocene marino del sottosuolo di Roma. Bollettino della Società Geologica Italiana 116, 435-451.

Coletti F., 2004. Note su alcuni vasi invetriati dai contesti medio e tardo imperiali del Santuario di Cibele sul Palatino, Archeologia Classica 55, 413-447.

Coletti F., 2012. La ceramica invetriata di età tardoantica a Roma. Nuovi dati da recenti scavi stratigrafici, Rei Cretariae

Romane Fautorum Acta 42, 181-191.

Coletti F., 2015. Un impianto manifatturiero per la lavorazione dei tessuti e i sistemi di approvvigionamento idrico del lato meridionale della Domus Tiberiana. Scienze dell'Antichità 21, 117-135.

Coletti F. and Margheritelli L., 2006. Ultime fasi di vita, abbandono e distruzione dei monumenti dell'area sud ovest del Palatino. Contesti stratigrafici e reperti, Scienze dell'Antichità 13, 465-497.

Cuomo di Caprio N., 2007. Ceramica Antiche tecniche di lavorazione e moderni metodi di indagine in Archeologia 2. L'erma di Bretschneider, Roma, pp. 752.

De Benedetto G.E., Laviano R., Sabbatini L., Zambonin P.G., 2002. Infrared spectroscopy in the mineralogical characterization of ancient pottery. Journal of Cultural Heritage 3, 177-186.

De Vito C., Medeghini L., Mignardi S., Orlandi D., Nigro L., Spagnoli F., Lottici P.P., Bersani D., 2014. Technological fingerprints of Black-Gloss Ware from Motya (Western Sicily, Italy). Applied Clay Science 88, 202-213.

De Vito C., Medeghini L., Mignardi S., Ballirano P., Peyronel L., 2015. Technological fingerprints of the Early Bronze Age clay figurines from Tell Mardikh-Ebla (Syria). Journal of the European Ceramic Society 35, 3743-3754.

De Vito C., Medeghini L., Mignardi S., Coletti F., Contino A., 2017. Roman glazed inkwells from the "Nuovo Mercato di Testaccio" (Rome, Italy): Production technology. Journal of the European Ceramic Society 37, 1779-1788.

De Vito C., Medeghini L., Garruto S., Coletti F., De Luca I., Mignardi S., 2018. Medieval glazed ceramic from Caesar's Forum (Rome, Italy): Production technology. Ceramics International 44, 5055-5062.

Di Luzio E., Fasani G.B., Bretschneider A., 2013. Potential rockfalls and analysis of slope dynamics in the Palatine archaeological area (Rome, Italy). Geologica Acta 11, 245-264.

Doménech-Carbó M.T., Doménech-Carbó A., Osete-Cortina L., Saurí-Peris M.C., 2006. A study on corrosion processes of archaeological glass from the Valencian Region (Spain) and its consolidation treatment. Microchimica Acta 154, 123-142.

Fabbri B., Gualtieri S., Shoval S., 2014. The presence of calcite in archeological ceramics. Journal of the European Ceramic Society 34, 1899-1911.

Forte V. and Medeghini L. 2017. A preliminary study of ceramic pastes in the copper age pottery production of the Rome area. Archaeological and Anthropological Sciences 9, 209-222.

Forte V., Cesaro, S.N., Medeghini L., 2018. Cooking traces on Copper Age pottery from central Italy: An integrated approach comprising use wear analysis, spectroscopic analysis and experimental archaeology. Journal of Archaeological Science: Reports 18, 121-138.

Funiciello R. and Giordano G., 2008a. La nuova carta geologica di Roma: litostratigrafia e organizzazione stratigrafica. In: La geologia di Roma. Dal centro storico alla periferia. Memorie descrittive della Carta geologica d'Italia. (Eds.): R. Funiciello, A. Praturlon, G. Giordano, Servizio Geologico d'Italia, 80, 39-86.

Funiciello R. and Giordano G., 2008b. Geological Map of Italy 1:50.000 scale, sheet 374 "Roma" and explanatory notes. Servizio Geologico d'Italia, Florence (Italy), Società Elaborazioni Cartografiche (S.E.L.C.A.).

Garofano I., Robador M.D., Perez-Rodriguez J.L., Castaing J., Pacheco C., Duran, A., 2015. Ceramics from the Alcazar Palace in Seville (Spain) dated between the 11th and 15th centuries: Compositions, technological features and degradation processes. Journal of the European Ceramic Society 35, 4307-4319.

Guarino V., De Bonis A., Faga I., Giampaola D., Grifa C., Langella A., Liuzza V., Pierobon R., Romano P., Morra V., 2016. Production and circulation of thin walled pottery from the Roman port of Neapolis, Campania (Italy). Periodico di Mineralogia 85, 95-114.

Hedges R.E.M., 1976. Pre-Islamic glazes in Mesopotamia-Nippur. Archaeometry 18, 209-213.

Legodi M.A. and de Wall D., 2007. Raman spectroscopic study of ancient South African domestic clay pottery. Spectrochimica Acta Part A 66, 135-142.

Lofrumento C., Zoppi A., Castellucci E.M., 2004. Micro-Raman spectroscopy of ancient ceramics: a study of French sigillata wares. Journal of Raman Spectroscopy 35, 650-655.

Madkour F., Imam H., Elsayed K., Meheina G. 2015. Elemental analysis study of glazes and ceramic bodies from Mamluk and Ottoman periods in Egypt by Laser-Induced Breakdown Spectroscopy (LIBS). Periodico di Mineralogia 84, 107-121.

Magrini C. and Sbarra F., 2005. Le ceramiche invetriate di Carlino. Nuovo contributo allo studio di una produzione antica, Ricerche di Archeologia altomedievale, medievale. Firenze, pp. 164.

Maniatis Y. and Tite M.S., 1981. Technological examination of Neolithic-Bronze Age pottery from central and southeast Europe and from the Near East. Journal of Archaeological Science 8, 59-76.

Marra F., Rosa C., De Rita D., Funiciello R., 1998. Stratigraphic and tectonic features of the Middle Pleistocene sedimentary and volcanic deposits in the area of Rome (Italy). Quaternary International 47-48, 51-63.

Mason R.B. and Tite M.S., 1997. The beginnings of tin-opacification of pottery glazes. Archaeometry 39, 41-58.

Medeghini L., Mignardi S., De Vito C., Bersani D., Lottici P.P., Turetta M., Sala M., Nigro L., 2013. Is Khirbet Kerak Ware from Khirbet al-Batrawy (Jordan) local or imported pottery?. Analytical Methods 5, 6622-6630.

Medeghini L., Fabrizi L., De Vito C., Mignardi S., Nigro L., Gallo E., Fiaccavento C., 2016a. The ceramic of the "Palace of the Copper Axes" (Khirbet al-Batrawy, Jordan): A palatial special production. Ceramics International 42, 5952-5962.

Medeghini L., Mignardi S., De Vito C., Conte A.M., 2016b. Evaluation of a FTIR data pretreatment method for Principal Component Analysis applied to archaeological ceramics. Microchemical Journal 125, 224-229.

Medeghini L., Mignardi S., De Vito C., Macro N., D'Andrea M., Richard S., 2016c. New insights on Early Bronze Age IV pottery production and consumption in the southern Levant: The case of Khirbat Iskandar, Jordan. Ceramics International 42, 18991-19005.

Medeghini L. and Nigro L., 2017. Khirbet al-Batrawy ceramics: a systematic mineralogical and petrographic study for investigating the material culture. Periodico di Mineralogia 86, 19-35.

Milli S., 1997. Depositional settings and high-frequency sequence stratigraphy of the middle-upper Pleistocene to Holocene deposits of the Roman basin. Geologica Romana 33, 99-136.

Molera J, Pradell T., Salvadò N., Vendrell-Saz M., 2001. Interaction between clay bodies and lead glazes. Journal of American Ceramic Society 84,1120-1128.

Molera J., Iñañez J.G., Molina G., Burch J., Alberch X., Glascock M.D., Pradell T., 2015. Lustre and glazed ceramic collection from Mas Llorens, 16-17th centuries (Salt, Girona). Provenance and technology. Periodico di Mineralogia 84, 45-63.

Moore P.R.S and Hedges R.E.M., 1975. Pre-Islamic ceramic glazes at Kish and Nineveh in Iraq. Archaeometry 17, 25-43.

Özçatal M., Yaygıngöl M., İssi A., Kara A., Turan S., Okyar F., Pfeiffer Taş S., Nastovad I., Grupče O., Minčeva-Šukarova B., 2014. Characterization of lead glazed potteries from Smyrna (Izmir/Turkey) using multiple analytical techniques; Part I: Glaze and engobe. Ceramics International 40, 2143-2151.

Papachristodoulou C., Oikonomou A., Ioannides K., Gravani K., 2006. A study of ancient pottery by means of X-ray fluorescence spectroscopy, multivariate statistics and mineralogical analysis. Analytica Chimica Acta 573, 347-353.

Quinn P.S., 2013. Ceramic Petrography: The interpretation of archaeological pottery and related artefacts in thin section. Archaeopress, Oxford, pp. 250.

Riccardi M.P., Messiga B., Duminuco P., 1999. An approach to the dynamics of clay firing. Applied Clay Science 15, 393-409.

Riederer J., 2004. Thin section microscopy applied to the study of archaeological ceramics. Hyperfine Interaction 154, 143-158.

Shoval S. and Nathan Y., 2011. Analyzing the calcination of sulfur-rich calcareous oil shales using FT-IR spectroscopy and applying curve-fitting technique. Journal of Thermal Analysis and Calorimetry 105, 883-896.

Shoval S. and Paz Y. 2015. Analyzing the fired-clay ceramic of EBA Canaanite pottery using FT-IR spectroscopy and LA-ICP-MS. Periodico di Mineralogia 84, 213-231.

Silvestri A., Molin G., Salviulo G., 2005. Archaeological glass alteration products in marine and land-based environments: morphological, chemical and microtextural characterization. Journal of Non Crystalline Solids 351, 1338-1349.

Tite M.S., 2008. Ceramic production, provenance and use-A review. Archaeometry 50, 216-231.

Tite M.S., Freestone I., Mason R., Molera J., Vendrell-Saz M., Wood N., 1998. Lead glazes in antiquity-methods of production and reasons for use. Archaeometry 40, 241-260.

Tite M.S., Kilikoglou V., Vekinis G., 2001. Strength, toughness and thermal shock resistance of ancient ceramics, and their influence on technological choice. Archaeometry 43, 301-324.

Tite M., Shortland A., Paynter S., 2002. The beginnings of vitreous materials in the Near East and Egypt. Accounts of Chemical Research 35, 585-593.

Trindade M.J., Dias M.I., Coroado J., Rocha F., 2009. Mineralogical transformations of calcareous rich clays with firing: a comparative study between calcite and dolomite rich clays from Algarve, Portugal. Applied Clay Science 42, 345-355.

Walton M.S. and Tite M., 2005. Le analisi sulla ceramica invetriata di Carlino. In: Le ceramiche invetriate di Carlino. Nuovo contributo allo studio di una produzione antica. (Eds.) C. Magrini, F. Sbarra, Ricerche di Archeologia altomedievale, medievale, Firenze, 67-68.

Walton M.S. and Tite M.S., 2010. Production technology of Roman lead glazed pottery and its continuance into late antiquity. Archaeometry 52, 733-759.

Whitbread I.K., 1995. Greek transport amphorae: a petrological and archaeological study. British School at Athens, Fitch Laboratory Occasional Paper 4, Athens, pp. 453.

Wolf S., Stos S., Mason R., Tite M.S., 2003. Lead isotope analyses of Islamic pottery glazes from Fustat, Egypt. Archaeometry 45, 405-420.